RSC Advances

ROYAL SOCIETY OF CHEMISTRY

www.rsc.org/advances

Cite this: DOI: 10.1039/c0xx00000x

www.rsc.org/xxxxxx

ARTICLE TYPE

Enhanced photocatalytic activity of the hierarchical structure TiO_2 hollow spheres with reactive (001) facets for the removal of toxic heavy metal Cr(VI)

Yong Yang,[a] Guozhong Wang,*[a] Quan Deng,[a] Huiming Wang,[a] Yunxia Zhang,[a] Dickon H.L. Ng[b] and Huijun Zhao[a,c]

Received (in XXX, XXX) Xth XXXXXXXXX 20XX, Accepted Xth XXXXXXXXX 20XX
DOI: 10.1039/b000000x

Hierarchical structure TiO_2 hollow spheres composed of nanometer-sized building blocks, nanoflakes with exposed anatase (001) facets, have been synthesized with a high yield through a facile fluoride-mediated hydrothermal route. The average diameter of the resultant TiO_2 hollow spheres was ~1 μm, and the width of well-crystallized anatase phase nanoflakes was ~50 nm. Nitrogen adsorption-desorption measurement revealed that the products had a high specific surface area of 26 m^2 g^{-1} and abundant mesoporous structure. The TiO_2 hollow spheres were used to photocatalytic degrade Cr(VI) in solution. The results indicated an enhanced photocatalytic activity compared to the other structured TiO_2, owing to the high specific surface area and abundant mesoporous properties of the TiO_2 hollow spheres, besides, the presence of the reactive (001) facets also contributed to the enhanced activity, it was found that the (001) facets were more effective in the absorption of Cr(VI) than the commonly exposed (101) facets, Besides, the surface fluorination of TiO_2 hollow spheres was found to have a negative role in the photocatalytic removal of Cr(VI). The TiO_2 hollow spheres not only could remove Cr(VI) from the wastewater, they also reduced the adsorbed toxic Cr(VI) to Cr(III) and further formed oxide or hydroxide. In addition, the TiO_2 hollow spheres photocatalysts with micron-scale size showed high durability in the cyclic tests.

Introduction

Water pollution caused by heavy metal ions have drawn intensive attention, among them, Cr(VI) was particularly hazardous owing to its acute toxicity to human and its high mobility in water.[1-6] Various techniques have been used to treat the Cr(VI), including ion exchange,[7] electrocoagulation,[8,9] membrane separation,[10] adsorption,[11,12] photocatalytic reduction.[13-15] Among these methods, ion exchange and membrane separation methods were not attractive because of their high operating costs, complicated procedures and harsh conditions. Electrocoagulation and adsorption methods are only able to transfer Cr(VI) but not effectively degrade its toxicity, and must be followed by some secondary treatments.[16] Heterogeneous photocatalytic reduction using semiconductor photocatalyst TiO_2 has been proposed as an economical and simple method for the removal of Cr(VI), especially for those with low concentration.[13-15]

The structural modification of the TiO_2 photocatalyst has been demonstrated to be an effective way to improve the photocatalytic activity. Comparing different TiO_2 structures (including nanoparticles, nanorods, and nanosheets), the TiO_2 hollow spheres structure have received considerable attention due to their low density, large surface area, good surface permeability and greater light-harvesting capacity.[17,18] It was reported that the TiO_2 hollow spheres showed enhanced photocatalytic activity compared to the commercially available nanometer-sized TiO_2 powders in the photodegradation of organic pollutant, such as acetone,[17,19] rhodamine B,[20] methyl orange[18] and the brilliant Red X3B.[21] The high specific surface area and aboundant mesoporous properties contributed to the enhanced photocatalytic activity, also with the micron meter sizes facilitated the recovery of the catalysts and great value in practical use.

On the other hand, the synthesis of reactive (001) facets exposed anatase TiO_2 single crystals has also been proved to be an alternative route to improve the photocatalytic efficiency of photocatalysts.[22-24] Numerous studies have suggested that the reactive (001) facets showed considerably enhanced photocatalytic activity towards the photocatalytic oxidation of organic pollutants. However, most of researches focused on the photocatalytic activity of the TiO_2 hollow spheres or the reactive (001) facets for the photodegradation of organic pollutant,[17-24] little attention was paid to the photocatalytic reduction removal of toxic heavy metal Cr(VI). The structural advantages of TiO_2 hollow spheres and reactive (001) facets should be expected to show a great potential in the photocatalytic reduction removal of Cr(VI). He et al. reported the use of reactive (001) facets exposed anatase TiO_2 nanosheets for the photocatalytic removal of Cr(VI), and the enhanced activity was demonstrated,[25] however, the

nanosheets tended to overlap with each other during the liquid phase photocatalysis, resulting in undesirable reduction in the specific surface area. It would be attractive to assemble the reactive (001) facets exposed TiO_2 nanosheets into micrometer-sized hierarchical hollow spheres structure and use them for the photocatalytic reduction removal of toxic heavy metal Cr(VI).

As to the synthesis of TiO_2 hollow spheres structure with reactive (001) facets, great efforts have been made by the researchers,[18,26,27] however, most of those reported synthesis methods either involve multiple complex reaction steps or require the use of extremely corrosive and toxic raw materials hydrofluoric acid. Here, we report the synthesis of micron-sized hierarchical structure TiO_2 hollow spheres with reactive (001) facets based on a facile fluoride-mediated strategy. The photocatalytic activity and durability of the TiO_2 hollow spheres in the removal of Cr(VI) are studied for the first time, the influence of surface fluorination and reactive (001) facets on the photocatalytic activity are also investigated and discussed in detail.

Experimental Section

Sample preparation

All reagents were commercial and used without further purification. Deionized water was used in the experiments. In a typical synthesis, 2 mmol of Titanium sulfate ($Ti(SO_4)_2$, ≥ 96.0%, Shang Hai Nan Hui Chemical Reagent Co. Ltd, CP) was dissolved into 40 mL mixed solution of the ammonium fluoride (NH_4F, Wu Xi Zhan Wang Chemical Reagent Co. Ltd, AR) and deionized water, and stirring for 3 h at room temperature. The molar ratio of fluorine to titanium (R_F) was 3. The mixed solution was transferred to a 70 mL Teflon-lined autoclave and maintained at 180 °C for 10 h. The white precipitates were collected, washed and rinsed with deionized water and ethanol, respectively, then dried in the oven at 70 °C for 8 h, the product was denoted as F-THS. While the TiO_2 hollow spheres composed of smaller crystallite size (denoted as SF-THS) were synthesized similar to the above process, except the addition of 4 mmol urea into the reaction solution, according to the previous work.[16] For the removal of the adsorbed fluorine ions on the surface of TiO_2, the sample was soaked into 0.1 M NaOH solution for 1 h, After rinsing with deionized water for several times until the pH value of the supernatant had attained a reading close to 7, then dried in the oven at 70 °C for 8 h. The samples of F-THS and SF-THS after removal of the adsorbed fluorine ions on the surface were denoted as THS and S-THS, respectively.

Characterization

The phases of the products were identified by X-ray diffraction analysis (XRD, Philips X'pert PRO) using Ni-filtered monochromatic CuK_α radiation at 40 keV and 40 mA. The morphology and structure of the products were characterized by a field emission scanning electron microscope (FESEM, Sirion 200 FEI) using an accelerating voltage of 5 kV, and a transmission electron microscopy (TEM, JEOL-2010, 200 kV) equipped with an energy dispersive X-ray spectrometer (EDX, Oxford, Link ISIS). The specific surface areas of the samples were determined by nitrogen adsorption (Micrometrics ASAP 2020M) at 77 K using the Brunauer–Emmett–Teller (BET) equation. The photoluminescence (PL) measurement was performed by using a LabRam confocal Raman microscope by JY Company. Samples were excited by the 325 nm line of acontinuous He–Cd laser at room temperature. X-ray photo electron spectroscopic (XPS) analyses were conducted on a Thermo Scientific ESCALAB250Xi system, equipped with a hemispherical energy analyser, an Al K_α X-ray source (hν=1486.6 eV) was operated with a base pressure of 3×10^{-8} Pa.

Photocatalytic activity evaluation

The evaluation of performance of photocatalysts for the removal of Cr(VI) in aqueous solutions was carried out at ambient condition. $K_2Cr_2O_7$ was used as the Cr(VI) sources. 40 mg photocatalyst was added into 80 mL of 10 mg/L Cr(VI) solution. The pH value of the reaction suspension was adjusted to 2.5–8.0 using HCl or NaOH. Only the optimum pH would be used in the further study. Before irradiation, the solution was stirred for 30 min in the dark to reach adsorption-desorption equilibrium between the photocatalyst and Cr(VI) solution. A 300 W high-pressure mercury lamp with maximum emission at 365 nm was used as the UV light source. At a given time interval of irradiation, 3 mL solution was taken out from the suspensions and centrifuged to remove the photocatalyst powder. The Cr(VI) concentration was monitored by the spectrophotometric method of the diphenylcarbazide at 540 nm using a spectrophotometer (CARY-5E). The total Cr ion concentrations in the solutions were measured by an inductively coupled plasma-optical emission spectrophotometer (ICP 6000 Thermal Electron).

After the first cycle, all the photocatalysts including the taken-out samples, were soaked in the 10% HNO_3 solution for 5 h before washing with deionized water and ethanol for several times, and were then dried at 70 °C for 8 h. The obtained powders were reused in the second and third cycles. The experimental process was similar to the above measurement of photocatalytic activity.

In the other set of experiments, the evaluation of photocatalytic degradation for the 20 mg/L (ppm) methyl orange and the 50 mg/L 2, 4-dichlorophenoxyacetic acid in water were performed with the similar procedures. The concentrations of methyl orange and 2, 4-dichlorophenoxyacetic acid were determined by the absorption peaks in UV-vis absorption spectra at the 464 and 282 nm peaks, respectively.

Results and Discussion

Characterization of the as-synthesized F-THS and SF-THS

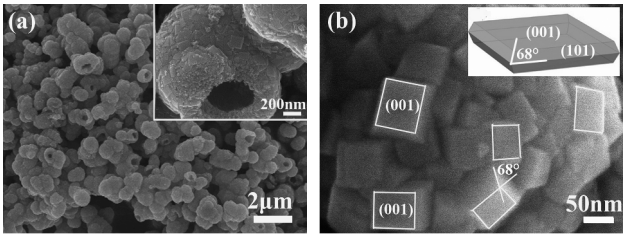

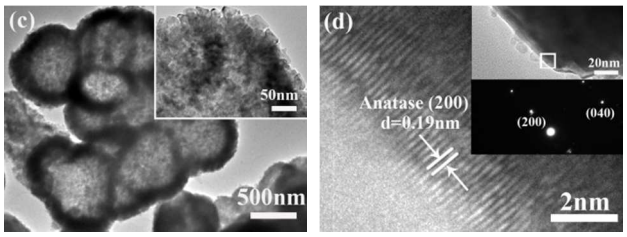

Figure 1. (a) and (b) FESEM images of F-THS, inset in (a) is the high-magnification image of a single sphere, and (b) is the schematic model of a highly truncated tetragonal bipyramid exposing (001) facets, respectively. (c) TEM image of F-THS, inset is the enlarged image and (d) HRTEM image and SAED pattern of the region highlighted by a rectangular box in the upper of inset (d).

The morphologies of the as-synthesized TiO_2 hollow spheres (denoted by F-THS) are shown in Figure 1. The field emission scanning electron microscope (FESEM) image (Figure 1a) of F-THS showed that the sample contained large quantities of spheres with a diameter of ~1 μm. The partial broken sphere displayed its interior and confirmed that they were hollow structure. From the high-magnification image of a single sphere (inset in Figure 1a), the external surface of the hollow sphere was rough and composed of randomly aggregated nanoflakes. The nanoflakes shared a similar shape with the reactive (001) facets exposed anatase single crystal, known as highly truncated tetragonal bipyramids (inset in Figure 1b). The enlarged FESEM image of the surface of a single sphere (Figure 1b) further confirmed the morphology of nanoflakes. The interfacial angles were determined to be around 68°, consistent with that between anatase (001) and (101) facets (inset in Figure 1b). Thus, the outside surfaces of nanoflakes could be indexed as (001) facets of anatase according to such shape symmetry. The transmission electron microscopy (TEM) image in Figure 1c clearly revealed the hollow spheres architecture of F-THS, and the nanoflakes inlaid on the external surfaces could be observed from the enlarged image in the inset of Figure 1c. In addition to the shape symmetry, the corresponding selected-area electron diffraction (SAED) pattern and high-resolution TEM (HRTEM) were further presented to reveal the crystallographic orientation of nanoflakes, shown in Figure 1d. The HRTEM image recorded perpendicular to the (001) facets showed spacing of 0.19 nm, representing the {200} atomic planes of anatase TiO_2.[22-24] Above results suggested that the outside surfaces of the nanoflakes could be indexed as the reactive (001) facet of anatase. The TiO_2 hollow spheres composed of smaller crystallite size (denoted as SF-THS) were also synthesized. The whole morphology of SF-THS (shown in Figure S1) was similar to that of F-THS, except that the building blocks of SF-THS were tiny nanoparticles with the size about 10 to 20 nm, which were much smaller than the reactive (001) facets exposed nanoflakes of F-THS.

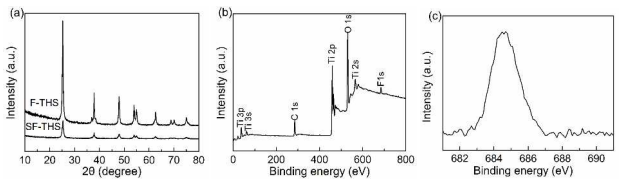

Figure 2. (a) XRD patterns of the different samples, (b) XPS survey spectrum of F-THS and (c) high-resolution XPS spectrum of the F 1s region of F-THS.

The XRD patterns of F-THS and SF-THS are shown in Figure 2a. All the peaks could be indexed as pure anatase phase of TiO_2 (JPCDS No. 21-1272). The peaks of F-THS were much narrower than that of SF-THS, indicating the increase in average crystal size and crystalline, which was consistent with the FESEM and TEM observation. In order to study the internal pore structures and specific surface areas of F-THS and SF-THS, the nitrogen adsorption-desorption measurement was performed (Figure S2). The isotherms of both F-THS and SF-THS were of type IV (Brunauer-Deming-Deming-Teller classification),[20] revealing the existence of abundant mesoporous structures. Using the BET equation, the specific surface area of F-THS and SF-THS were evaluated to be about 26, 125 $m^2\ g^{-1}$, respectively. Figure 2b shows the XPS survey spectrum of F-THS. In addition to the peaks of Ti, O and C (the C element is mainly ascribed to the contamination from XPS instrument itself and the carbon dioxide in the air), a peak at 684.6 eV (Figure 2c) was found, corresponding to that of F adsorbed on the surface of TiO_2 (≡Ti-F). No signal for F^- in the lattice of TiO_2 (bonding energy is equal to 688.5 eV) was detected.[21] The surface fluorination was caused by a simple ligand exchange reaction between surface hydroxyl groups on TiO_2 and fluoride anions (F^-) due to the high F–Ti bonding energy.[18]

Further study indicated that the molar ratio of fluorine to titanium (denoted by R_F) in the reaction solutions had a significant effect on the formation of F-THS (shown in Figure S3). When the value of R_F was equal to 0, i.e., without the addition of fluoride, the products were solid spherical aggregates (Figure S3a). When R_F equaled to 0.5 or 1, a small amount of broken microspheres displaying hollow interior was observed (Figure S3b and S3c). When the R_F increased to 2, large quantities of hollow spheres similar to F-THS were obtained (Figure S3d). When the fluoride concentration further increased (R_F = 5), the product was solid microspheres composed of randomly aggregated nanoflakes (Figure S3e) instead of hollow microspheres. According to the previous works by Yu et al,[17,20,28] the formation of F-THS was a fluoride-mediated self-transformation process, which was proven to be an effective route for the synthesis of hollow spheres structured TiO_2. Besides, the synthesis of anatase TiO_2 with (001) facets through the assistant of fluoride had also been reported.[22-24] In this work, proper fluoride concentration (R_F = 3) not only favored the crystallization of anatase during the formation of hollow sphere, but also induced the formation of reactive (001) facets.[22-24] Especially, the addition of urea could tune the nucleation dynamics of the elementary TiO_2 building blocks and inhibited the progressive crystal growth,[28] SF-THS was finally obtained and composed of small nanoparticles.

Optimal pH value on the photocatalytic removal of Cr(VI)

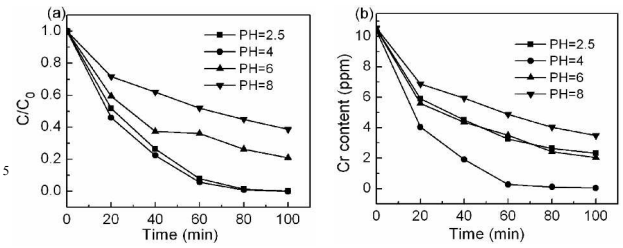

Figure 3. (a) Cr(VI) normalization concentration and (b) the total Cr ions concentration in the solutions versus the exposure time under irradiation with the different initial pH values. C_0 is the initial concentration of Cr(VI), C is concentration of the remaining Cr(VI) at time t. Cr(VI) concentration was measured by the spectrophotometric method of the diphenylcarbazide at 540 nm, the total Cr ions concentration was measured by an inductively coupled plasma (ICP)-optical emission spectrophotometer.

The influence of pH value on the photocatalytic activity of F-THS for the Cr(VI) removal is shown in Figure 3a. Cr(VI) was completely removed under the UV light irradiation in 100 min with pH values of 2.5 and 4, while the removal efficiency of Cr(VI) decreased swiftly with the pH value increasing over 4. The possible reason was that the potential difference between the conduction band of TiO_2 and Cr(VI)/Cr(III) increased with the pH decreasing, thus the thermodynamic driving force for the reduction of Cr(VI) was enhanced at low pH.[15] On the other hand, the zero charge point of TiO_2 was about pH = 6.25. In acidic condition, the surface of TiO_2 was mainly of positive charge. Therefore, the lower pH was favourable for the adsorption of negatively charged Cr(VI) groups on TiO_2 due to the electrostatic attraction, and consequently enhanced the Cr(VI) removal. In the high pH region, there would be an electrostatic repulsion between negatively charged group (CrO_4^{2-} or $Cr_2O_7^{2-}$) and TiO_2, resulting in the decrease in the adsorption.[13] It should be mentioned that the total Cr ions concentration in the solution measured by ICP did not decrease to zero under the UV light irradiation for 100 min with the pH of 2.5 (Figure 3b), there was still a total of 2.33 ppm Cr ions remained in the solution. This indicated that Cr(VI) ions were initially photocatalytic reduced to Cr(III) ions by F-THS, and then desorbed into the solution due to the low adsorption capacity for Cr(III) on the surface of F-THS at this pH value.[29] However, this phenomena of the desorption of Cr(III) ions was not found in condition with pH = 4, the total concentration of Cr ions was found to be about 0.048 ppm after 100 min, which was slightly lower than the allowable limit of 0.05 ppm in the drinking water in countries like Sweden and Germany.[11] Based on the above results we proposed that the optimal pH value of the TiO_2 catalyst for the photocatalytic removal of Cr(VI) was around 4.

Effect of surface fluorination on the photocatalytic activity

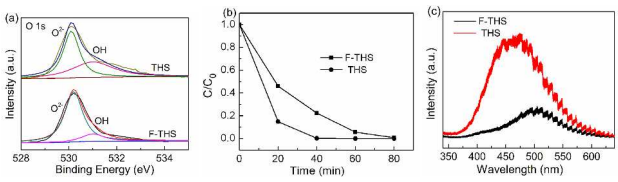

Figure 4. (a) High-resolution XPS spectra of O 1s region of the different TiO_2 powder, (b) Cr(VI) normalization concentration versus the exposure time under irradiation with the different TiO_2 photocatalysts. C_0 is the initial concentration of Cr(VI), C is concentration of the remaining Cr(VI) at time t. (c) Photoluminescence spectra of the different TiO_2 powder.

The effect of fluorine on the photocatalytic activity of TiO_2 in the photodegradation of organic pollutant was widely investigated,[17-21] however, for the removal of heavy metal Cr(VI) was rarely reported.[25] In order to investigate the influence of surface fluorination on the photocatalytic degradation of Cr(VI), the surface-bonded fluoride species of F-THS were removed by NaOH washing (see the experimental section for details) without the change of morphology and structure, clean (001) facets could be obtained as reported,[30,31] the sample of F-THS after NaOH washing was denoted by THS. XPS was used to characterize the surface chemical compositions of F-THS and THS (Figure 4a). It appeared that the ratio of OH (at about 531.0 eV) to O^{2-} (at about 530.0 eV) in the O 1s spectra of THS had increased more significantly than that of F-THS, indicating a replacement of the surface-bonded fluoride species by hydroxyl groups due to NaOH washing.[32] In addition, the photocatalytic activity of THS for the removal of Cr(VI) was investigated at pH = 4. The photocatalytic degradation rate of THS was found much faster than that of F-THS (Figure 4b), demonstrating that the surface fluorination hindered the photocatalytic activity. The result was in contrary with the previous reports that the surface fluorination could significantly enhance the photocatalytic degradation of organic anionic, cationic, neutral pollutant.[17-21] The photocatalytic activity of F-THS in the photo-degradation of organic pollutant as methyl orange and 2, 4-dichlorophenoxyacetic acid was hindered after the removal of the surface fluorination by NaOH washing (shown in Figure S4), indicating that the surface fluorination was indeed beneficial to the photocatalytic degradation of organic pollutant. The negative role of surface fluorination for the photocatalytic removal of Cr(VI) might be originated from the following two sources. First, there were more surface hydroxyl group of THS due to the replacement of the surface-bonded fluoride species by NaOH washing, and this might play a decisive role in the photocatalytic reduction removal of Cr(VI).[25,32] Second, it was reported that surface Ti-F group could act as an electron-trapping sites to trap the photo-generated electrons and transferring them to O_2 adsorbed on the surface of TiO_2, thus enhanced the separation of electrons and holes.[20,33] In our work, the effect of fluorination on the recombination of photo-generated electron/hole pairs of the samples was measured by the PL emission (shown in Figure 4c). The intensity of PL spectra of F-THS was much lower than that of THS, indicating that a better separation efficiency of electrons and holes could indeed be achieved by the surface fluorination.[14] However, the difference was that the photocatalytic degradation of organic pollutant mainly relied on the photo-generated holes, while the photocatalytic reduction of Cr(VI) needed the participation of photo-generated electrons. The trapping of photo-generated electrons by the surface Ti-F group would hinder the transferring of electrons to Cr(VI), thus was detrimental to the photocatalytic reduction of Cr(VI). Our result was different from the previous work which reported that the surface fluorination was beneficial to the photocatalytic removal of Cr(VI),[25] because part of the surface-bonded fluoride species in that work was substitutional F atoms in TiO_2 crystal lattice, but in our work the surface-bonded

fluoride species was wholly surface-absorbed F(≡ Ti-F). Investigated work also showed that similar experiment of the photocatalytic activity of SF-THS for degradation of Cr(VI) was enhanced after removal of surface fluorination by NaOH washing (Figure S5, the sample of the SF-THS after NaOH washing was denoted by S-THS). All these above results pointed to the fact that the surface fluorination of TiO_2 hollow spheres hindered the photocatalytic removal of Cr(VI).

Structurally enhanced the photocatalytic activity

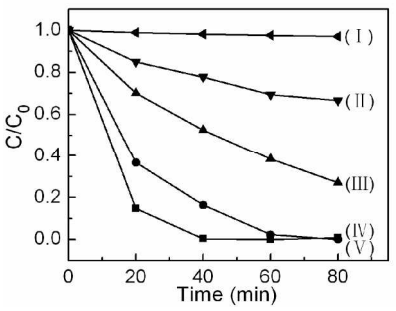

Figure 5. Cr(VI) normalization concentration versus the exposure time under irradiation with the different TiO_2 catalysts: (I) without catalysts; (II) micron-sized TiO_2 powder; (III) nanometer-sized TiO_2 powder; (IV) S-THS and (V) THS.

Table 1. BET specific surface area and apparent rate constant data k_{app} of the different TiO_2 photocatalysts.

Sample	THS	S-THS	micron-sized TiO_2	nanometer-sized TiO_2
BET ($m^2\ g^{-1}$)	26	125	2.2	60
k_{app} (min^{-1})	0.0867	0.0516	0.0051	0.0161

The photocatalytic activity of the commercial anatase micron-sized and nanometer-sized TiO_2 powder (see Figure S6) was selected as the standard references in the evaluation of the removal ability for Cr(VI). Figure 5 shows the photocatalytic performance for the Cr(VI) removal with the different TiO_2 photocatalysts at the pH level of 4. Without the addition of photocatalyst, the Cr(VI) removal could not be observed under irradiation (curve (I) in Figure 5). The THS and S-THS with hierarchical structure exhibited high photocatalytic activity than that of mono-morphological commercial anatase micron-sized and nanometer-sized TiO_2 powders, as shown in Figure 5. Within relatively low Cr(VI) concentration, their photocatalytic process and reaction kinetics could be expressed by a pseudo-first-order reaction and an apparent rate constant k_{app} (shown in Table 1). The k_{app} of THS was nearly 6 and 18 times larger than that of the nanometer-sized TiO_2 and micron-sized TiO_2, respectively. The k_{app} of S-THS was also larger than that of the nanometer-sized TiO_2 and micron-sized TiO_2 with a factor of about 3 and 6 times, respectively. This enhanced photocatalytic performance of THS and S-THS could be described as the structure-induced enhancement,[34,35] attributed to the high specific surface area and abundant mesoporous properties of the TiO_2 hollow spheres, which could provide ideal channels for easy and fast diffusion of the Cr(VI) molecules to contact the TiO_2 building blocks.[34] Moreover, the enhanced light harvesting abilities owing to the special hollow structures of THS and S-THS would increase the quantity of photo-generated electrons and holes to participate in the photocatalytic reactions.[16] Also we have presented the systematic comparison experiment to study the photocatalytic efficiency of the commercial photocatalyst Degussa P25 (see Figure S7 in the supporting information), it was found that the photocatalytic efficiency of Degussa P25 was much lower than that of the as-synthesized hierarchical structure TiO_2 hollow spheres, indicating enhanced activity of the TiO_2 hollow spheres in photocatalytic removal of Cr(VI).

The morphology of THS before and after treating the Cr(VI) solution was examined by TEM (Figure S8a), there was no obvious morphology change in the hollow spheres structure. The element analysis of energy dispersive X-ray spectrometer (EDX) revealed that Ti, Cr, O, C and Cu elements co-existed on the surface of THS after treating the Cr(VI) solution (Figure S8b). Among them, Ti and O signals were originated from TiO_2 crystals, the C signal was from the carbon film, and Cu was from the copper grid. The spatial distribution of the different compositional elements was clarified by elemental mapping (Figure S8c-S8e). The spatial distribution of Cr was similar to the distribution of Ti and O, indicating that THS was an effective photocatalyst for the removal of Cr(VI).

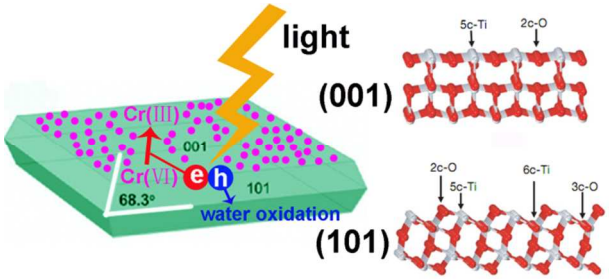

Figure 6. Schematic illustration of the photocatalytic removal of Cr(VI) with reactive (001) facets and the atomic structures of clean (001) and (101) surfaces. Cr(VI) molecules are represented by purple spheres. Ti and O atoms are represented by grey and red spheres, with six-fold Ti, five-fold Ti, three-fold O and two-fold O labelled as 6c-Ti, 5c-Ti, 3c-O and 2c-O, respectively.

It was worth noting that THS showed the best photocatalytic performance, but its specific surface area was much lower than that of S-THS and nanometer-sized TiO_2 powders (shown in Table 1). This indicated that the specific surface area was an important factor influencing the photocatalytic activity, but was not the only one. Since THS and S-THS had the similar preparation condition and the morphology, the presence of reactive (001) facets in THS might contribute significantly to the observed high photocatalytic activity. Reactive (001) facets of THS with 100% five coordinate unsaturated linkage Ti atoms (5c-Ti) were more beneficial to the absorption of negatively charged Cr(VI),[36] in contrast to the normally exposed (101) facets with only 50% unsaturated linkage Ti atoms (Figure 6). Besides, according to some previous reports,[22,25] the synergism of reactive (001) facet and (101) facet in THS might induce the selective migration of photo-generated electrons and holes to the specific exposed crystal facets, which would hinder the recombination rate of photo-generated electrons and holes and thus enhance the

photocatalytic activity (Figure 6). In the present study, we found that the F-THS with reactive (001) facets showed much lower dark adsorption ability of Cr(VI) than that of SF-THS. After 30 min of dark adsorption for F-THS and SF-THS, the Cr(VI) removal efficiencies were 1.6% and 5.3%, respectively, due to the surface fluorination that hindered the activity of (001) facets. When the surface fluorination was removed through NaOH washing, the excellent adsorption ability of THS with clean reactive (001) facets was fully reflected, exceeding that of S-THS (the Cr(VI) removal efficiencies after 30 min of dark adsorption for THS and S-THS were 9.8% and 7.1%, respectively). The results indicated that reactive (001) facets were indeed more beneficial to the absorption of negatively charged Cr(VI). Moreover, the reactive (001) facets exposed nanosheets were also synthesized by the previous method,[37] which were used to investigate the activity of the different crystal facets in the photocatalytic removal of Cr(VI) compared to THS. Figure S9 shows the TEM images of the nanosheets after treating the Cr(VI) solution, there were many Cr species wrapped around the nanosheets, especially around the (001) facets (Figure S9c). The Cr species contents were analyzed by EDX, the content of Cr species absorbed on the (001) facets (EDX recorded from [001] direction) were about three times higher than that of the (101) facets (EDX recorded from [100] direction), indicating that the reactive (001) facets indeed had higher activity in the photocatalytic removal of Cr(VI). The detail evidence was under investigation.

XPS was used to further study the absorbed Cr species on the surface of THS after photocatalytic reaction. Figure S10 shows the corresponding high-resolution XPS spectra of the Cr 2p region. The broad peak of Cr $2p^{3/2}$ could be fitted to two main peaks of 576.5, and 577.6 eV, consistent with the reported XPS spectra for oxides or the hydroxide of characteristics Cr(III) (e.g. $Cr(III)_xO_y$ and $Cr(OH)_3$), a weak peak at 579.6 eV corresponded to the characteristics binding energy of adsorbed Cr^{6+} ions.[38,39] This suggested that the photocatalytic process of Cr(VI) was as follows: Cr(VI) ions was first adsorbed on the surface of THS and then reduced to Cr(III) species by the photo-excited electrons, and finally deposited on the surface of THS.

The capacity of photocatalyst THS for the removal of Cr(VI) was also investigated (Figure S11). The removal efficiency could still reach 50% and 70% after 4 h of UV light irradiation with 0.1 and 0.3 g/L THS, respectively, indicating that each gram of THS could eliminate up to 50 mg of Cr(VI) from water. It was higher than that of the reported Fe_3O_4 micron-spheres and mesoporous titania beads,[16,32] and the removal time here was much shorter.

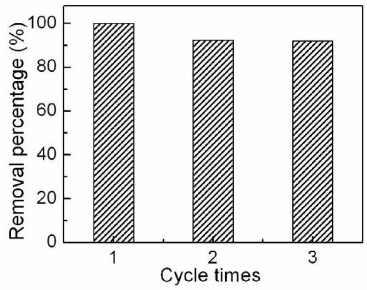

Figure 7. Durability of THS under the UV light irradiation for the three cycles.

In addition to the photocatalytic activity, the stability and recycle of the photocatalyst were also important in practical applications. In the present study, the durability of the photocatalytic activity of THS was studied by reusing of the catalysts in fresh Cr(VI) solution under the UV light irradiation. Figure 7 shows the photocatalytic ability of the THS for three cycles (40 min irradiation for each cycle). It was found that the removal percentage of Cr(VI) after three cycles could still reach 92%, indicating the feasibility of regeneration of THS.

Conclusions

Hierarchical structure TiO_2 hollow spheres with reactive (001) facets were hydrothermal synthesized with a high yield based on the fluoride-mediated self-transformation strategy. The photocatalytic evaluation in the removal of heavy metal Cr(VI) suggested that surface fluorination of TiO_2 hollow spheres played a negative role to the photocatalytic activity. When the surface fluorine of TiO_2 hollow spheres was removed, a considerably enhanced photocatalytic activity was achieved comparing to the other structured TiO_2 powders, the hierarchical structure (high specific surface area and aboundant mesoporous properties) together with the reactive (001) facets contributed to the enhanced photocatalytic activity. Further characterization results suggested that TiO_2 hollow spheres not only removed Cr(VI) from the wastewater, but also reduced the adsorbed toxic Cr(VI) to low toxic Cr(III) and further formed oxide or hydroxide. Moreover, TiO_2 hollow spheres could be regenerated. This work not only enriched the application of TiO_2 hollow spheres in the photocatalytic treatment of Cr(VI), but also revealed the double-sided nature of the surface fluorination. However, the relationship between the exposed reactive (001) facets and the enhanced photocatalytic activity towards Cr(VI) needs to be further studied. The as-synthesized hierarchical structure TiO_2 hollow spheres are also of great interest in the removal of other environmental pollutants.

Acknowledgment

This work was supported by the National Basic Research Program of China (Grant No. 2013CB934302), the Natural Science Foundation of China (Grant No. 51072199, 21177132 and 51272255), and Strategic Priority Research Program of the Chinese Academy of Sciences (Grant No. XDA09030200).

Notes and references

[a] *Key Laboratory of Materials Physics, Centre for Environmental and Energy Nanomaterials, Anhui Key Laboratory of Nanomaterials and Nanotechnology, Institute of Solid State Physics, Chinese Academy of Sciences, P.O. Box 1129, Hefei 230031, P.R. China. Fax: (86) 0551-65591434; Tel: (86) 0551-65595616; E-mail: gzhwang@issp.ac.cn*
[b] *Department of Physics, The Chinese University of Hong Kong, Shatin, Hong Kong*
[c] *Centre for Clean Environment and Energy, Gold Coast Campus, Griffith University, Queensland 4222, Australia*

†Electronic Supplementary Information (ESI) available: Additional figures including FESEM image, optical absorbance spectra, TEM image, XPS spectra, and so on. See DOI: 10.1039/b000000x/

1 S. X. Liu, *Bull. Environ. Contam. Toxicol.*, 2005, **74**, 706.

2 L. M. Wang, N. Wang, L. H. Zhu, H. W. Yu and H. Q. Tang, *J. Hazard. Mater.*, 2008, **152**, 93.
3 M. Rivero and W. D. Marshall, *J. Hazard. Mater.*, 2009, **169**, 1081.
4 M. V. Dozzi, A. Saccomanni and E. Selli, *J. Hazard. Mater.*, 2012, **211**, 188.
5 R. L. Qiu, D. D. Zhang, Z. H. Diao, X. F. Huang, C. He, J. L. Morel and Y. Xiong, *Water Res.*, 2012, **46**, 2299.
6 X. W. Zhao and L. M. Qi, *Nanotechnology*, 2012, **23**, 235604.
7 Y. Q. Xing, X. M. Chen and D. H. Wang, *Environ. Sci. Technol.*, 2007, **41**, 1439.
8 I. Heidmann and W. Calmano, *J. Hazard. Mater.*, 2008, **152**, 934.
9 P. Gao, X. M. Chen, F. Shen and G. H. Chen, *Sep. Purif. Technol.*, 2005, **43**, 117.
10 R. Guell, E. Antico, V. Salvado and C. Fontas, *Sep. Purif. Technol.*, 2008, **62**, 389.
11 S. Mor, K. Ravindra and N. R. *Bishnoi, Bioresour. Technol.*, 2007, **98**, 954.
12 M. E. R. Carmona, M. A. P. Silva and S. G. F. Leite, *Process Biochem.*, 2005, **40**, 779.
13 J. W. Fan, X. H. Liu and J. Zhang, *Environ. Technol.*, 2011, **32**, 427.
14 X. J. Liu, L. K. Pan, T. Lv, G. Zhu, T. Lu, Z. Sun and C. Q. Sun, *Rsc Adv., 2011,* **1**, 1245.
15 J. K. Yang, S. M. Lee, M. Farrokhi, O. Giahi and M. S. Siboni, *Desalin. Water Treat.*, 2012, **46**, 375.
16 G. Liu, Q. Deng, H. M. Wang, S. H. Kang, Y. Yang, D. H. L. Ng, W. P. Cai and G. Z. Wang, *Chem. Eur. J.*, 2012, **18**, 13418.
17 J. G. Yu, S. W. Liu and H. G. Yu, *J. Catal.*, 2007, **249**, 59.
18 J. Q. Li, D. F. Wang, H. I. Liu, Z. L. He and Z. F. Zhu, *Appl. Surf. Sci.*, 2011, **257**, 5879.
19 J. G. Yu and J. Zhang, *Dalton Trans., 2010,* **39**, 5860.
20 J. G. Yu, Q. J. Xiang, J. R. Ran and S. Mann, *CrystEngComm, 2010,* **12**, 872.
21 M. Liu, K. L. Lv, G. H. Wang, Z. Y. Wang, Y. X. Zhao and Y. R. Deng, *Chem. Eng. Technol.*, 2010, **33**, 1531.
22 S. W. Liu, J. G. Yu and M. Jaroniec, *Chem. Mater.*, 2011, **23**, 4085.
23 D. Q. Zhang, G. S. Li, X. F. Yang and J. C. Yu. *Chem. Commun., 2009,* 4381.
24 H. G. Yang, C. H. Sun, S. Z. Qiao, J. Zou, G. Liu, S. C. Smith, H. M. Cheng and G. Q. Lu, *Nature, 2008,* **453**, 638.
25 Z. Q. He, Q. L. Cai, M. Wu, Y. Q. Shi, H. Y. Fang, L. D. Li, J. C. Chen, J. M. Chen and S. Song, *Ind. Eng. Chem. Res.*, 2013, **52**, 9556.
26 S. J. Ding, J. S. Chen, Z. Y. Wang, Y. L. Cheah, S. Madhavi, X. A. Hu and X. W. Lou, *J. Mater. Chem.,* 2011, **21**, 1677.
27 X. L. Wang, H. L. He, Y. Chen, J. Q. Zhao and X. Y. Zhang, *Appl. Surf. Sci.*, 2012, **258**, 5863.
28 S. W. Liu, J. G. Yu and S. Mann, *Nanotechnology*, 2009, **20**, 325606.
29 S. C. Xu, Y. X. Zhang, S. S. Pan, H. L. Ding and G. H. Li, *J. Hazard. Mater.*, 2011, **196**, 29.
30 S. W. Liu, J. G. Yu and M. Jaroniec, *J. Am. Chem. Soc., 2010,* **132**, 11914.
31 Z. Y. Wang, K. L. Lv, G. H. Wang, K. J. Deng and D. G. Tang, *Appl. Catal., B: Environ.,* 2010, **100**, 378.
32 N. Wu, H. H. Wei and L. Z. Zhang, *Environ. Sci. Technol.*, 2012, **46**, 419.
33 J. G. Yu, W. G. Wang, B. Cheng and B. L. Su, *J. Phys. Chem. C, 2009,* **113**, 6743.
34 X. W. Duan, G. Z. Wang, H. Q. Wang, Y. Q. Wang, C. Shen and W. P. Cai, *CrystEngComm., 2010,* **12**, 2821.
35 F. Lu, W. P. Cai and Y. G. Zhang, *Adv. Funct. Mater.*, 2008, **18**, 1047.
36 J. Pan, G. Liu, G. Q. Lu and H. M. Cheng, *Angew. Chem. Int. Ed.*, 2011, **50**, 2133.
37 Z. Y. Wang, K. L. Lv, G. H. Wang, K. J. Deng and D. G. Tang. *Appl. Catal., B: Environ.,* 2010, **100**, 378.
38 *M. Mullet, F. Demoisson, B. Humbert, L. J. Michot and D.,Vantelon, Geochim. Cosmochim. Acta*., 2007, **71**, 3257.
39 D. Shuttleworth, *J. Phys. Chem.*, 1980, **84**, 1629.